4

The formation and evolution of layered structures in Hele-Shaw cells

Abstract

Horizontally layered structures can develop in porous or partially molten environments, such as magma chambers, the early Earth's mantle, and hydrothermal systems. The processes that bring about the formation and evolution of these layers are investigated with a numerical model of convection in a Hele-Shaw cell, in which a compositionally stably stratified fluid is heated from below. Growth of a convective layer at the bottom of the domain through entrainment, the formation of a horizontal density interface on top of this layer and destabilization of the next layer are closely coupled. It is shown that the growth of the first convective layer stops once the thermal equilibrium is reached. Since heat (solute) transfer across the thin density interfaces becomes purely diffusive (dispersive), the separately convecting layers can persist on a compositionally dispersive time scale. While the number of layers that develop is determined by the magnitude of the thermal Rayleigh number, the final height of a newly formed layer is inversely proportional to the buoyancy ratio. Two dynamical mechanisms which lead to sudden interface disappearance determine the vertical layer scales, rather than the initial evolution toward the thermal equilibrium.

4.1 Introduction

Among all geological structures, layering is probably one of the most common on nearly every scale. Horizontally layered structures vary from relatively small scales like in magmatic intrusions [*Cawthorn*, 1996] to the global scale structures of planetary interiors [*Stevenson*, 1989; *Olson et al.*, 1990]. Beyond geological settings, layer formation plays a role in the oceans and for the evolution of hydrothermal systems [*Griffiths*, 1981; *Bischoff and Rosenbauer*, 1989; *Fournier*, 1990; *Williams*, 1997].

Double-diffusive convection (DDC) in pure viscous fluids (in the following referred to as free flow, in contrast to flow in porous media) has been proposed to be a prominent layer forming mechanism in the oceans [*Schmitt*, 1994] and, later, in magma chambers [*McBirney*

This chapter has been published as Schoofs, S., Trompert, R. A., and U. Hansen, The formation and evolution of layered structures in porous media, *J. Geophys. Res., 103*, 20843-20858, 1998.

and Noyes, 1979; *Spera et al.*, 1986; *Hansen and Yuen*, 1995]. This layer formation mechanism may have played a role also during the evolution of the moon [*Alley and Parmentier*, 1998]. DDC is a fluid dynamical phenomenon, where two components with different diffusivities (e.g., heat and compositional concentration of dissolved elements) are the sources of buoyancy.

In the geological settings, however, layered structures often develop in a porous or partially molten magma environment [*Stevenson*, 1989], rather than in a purely viscous fluid one. Therefore we are interested in the formation and evolution of these layered structures in partially molten systems. As a first-order approximation, these systems can be represented by a rigid porous medium [*Aharonov et al.*, 1997], of which the porosity ϕ is typically as small as a few volume per cents. We consider the case where destabilization is accomplished by imposing a positive temperature contrast at the bottom, while the compositional concentration is initially stably stratified. This case is equivalent to the case of cooling a compositionally stable stratification from the top. Other layer-forming mechanisms, like sidewall heating of a stable compositional stratification [*Kranenborg*, 1997], are beyond the scope of this study.

DDC in a porous medium has been treated both analytically and experimentally in previous studies and was reviewed by *Nield and Bejan* [1992]. The dynamics of DDC in porous media differs in a number of ways from that of free flow. Evidently, the most prominent difference is the presence of the solid state. which leads to a retardation of heat as compared to solute (see also Chapter 7). In order to reveal the basic features of the layer formation in porous media, the model which is employed here resembles that of a Hele-Shaw cell. With this assumption, the dynamics differ from flow in a natural porous medium by the fact that heat and solute advect at the same velocity through the medium ($\phi^* = 1$ in equation 2.18). In Chapter 5, the layer-forming mechanism is studied in a more realistic (but numerically more challenging) medium with $\phi^* < 1$.

Another difference from free flow is that the drag force, exerted by the solid matrix, dominates over viscous forces in porous media flow. Moreover, inertial forces are negligible, which reduces the possibility of entraining nonbuoyant fluid from a density gradient into a convecting region. Finally, due to the lack of advection or diffusion of vorticity, the flow geometry produced by convection is different from free flow: slender cells connect the horizontal boundaries of the domain. As a result, vertical transport of heat and solute is very efficient. In general, DDC of a fluid in a porous medium takes the form of a boundary layer flow [*Nield and Bejan*, 1992]. Laboratory experiments in porous media showed that a thin density interface between two convective layers can be maintained against diffusive thickening [*Griffiths*, 1981], which is essential for the persistence of individual layers.

Studies on layer formation in free flow showed that the growth of the convective layer is limited by the development of a stable buoyancy jump on top of the convective layer, while the next layer is destabilized by considerable heat flux through this interface [*Fernando*, 1987; *Molemaker and Dijkstra*, 1997]. At present, it is unclear if and what extent these mechanisms work in partially solidified and porous systems. In order to address these questions, the results from computations with a numerical model of convection in a Hele-Shaw cell are presented here. Besides the layer forming mechanism, typical time and spatial scales of layer formation will be discussed.

The outline of this chapter is as follows. First, the model setup is given. In section 4.3, the results of a number of simulations with various Rayleigh numbers and buoyancy ratios are described. Focus is on the generation of the separately convecting layers, the mechanism of limitation of the layer heights, the sensitivity to parameter and initial conditions and, finally, on possible mechanisms of intermittent changes of the layer structures. Finally, the results are summarized in section 4.4.

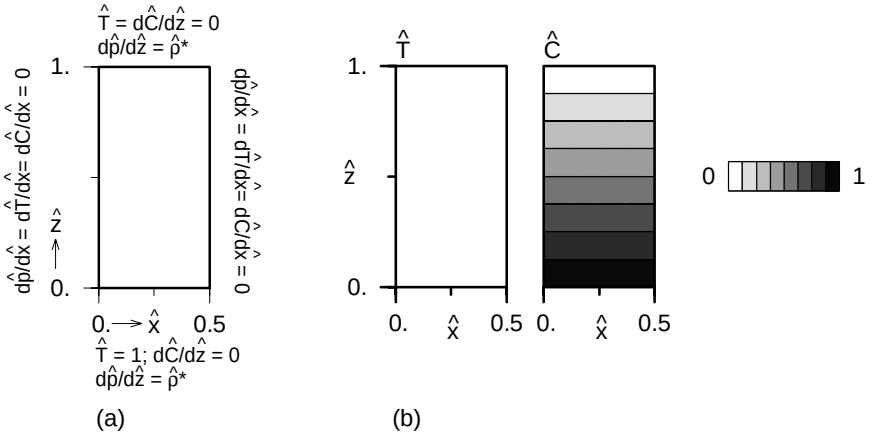

Figure 4.1: (a) Geometrical setup and boundary conditions of the experiment in the porous medium and (b) initial conditions.

4.2 Model setup

A two-dimensional homogeneous porous medium is considered, which is saturated with fluid. The system of equations used in this chapter consists of equations (2.16), (2.17) and (2.18). The thermal diffusivity is taken 100 times higher than the effective dispersion of compositional concentration ($Le_{\text{eff}} = 100$). This is a reasonable value both for magmatic and water-heat-salt systems. To reveal the fundamental features of the layer formation, it is assumed that heat and solute advect at the same velocity through the medium ($\phi^* = 1$ in equation 2.18). The numerical model used in this chapter resembles a Hele-Shaw cell (for a description, see Chapter 1). In this approximation, the inertial fluid acceleration is virtually negligible for the viscous motion. The dynamics governing the convection reduce to a force balance between pressure, friction and buoyancy (Darcy's law, equation (2.2)) [*Shen and Veronis*, 1991].

The model is set up in a rectangular domain of aspect ratio $A = 0.5$ with impermeable boundaries (see Figure 4.1a). A thermal contrast is imposed at the bottom, while the temperature at the top is fixed to zero. The vertical walls are insulators with respect to heat transport, while all sides satisfy no-flux conditions for the solute. Initially, the motionless interior is cold and the solute concentration is stably stratified, having a linear gradient $\partial\hat{C}/\partial\hat{z} = 1$ (Figure 4.1b). In dimensionless form, the boundary and initial conditions are defined as:

$$
\begin{aligned}
&\hat{x} = 0, A: && \partial\hat{p}/\partial\hat{x} = \partial\hat{T}/\partial\hat{x} = \partial\hat{C}/\partial\hat{x} = 0,\\
&\hat{z} = 0: && \partial\hat{p}/\partial\hat{z} = \hat{\rho}^*;\ \hat{T} = 1;\ \partial\hat{C}/\partial\hat{z} = 0,\\
&\hat{z} = 1: && \partial\hat{p}/\partial\hat{z} = \hat{\rho}^*;\ \hat{T} = 0;\ \partial\hat{C}/\partial\hat{z} = 0,\\
&\hat{t} = 0: && \hat{T} = 0;\ \partial\hat{C}/\partial\hat{z} = 1.
\end{aligned}
$$

In the parameter range appropriate for layer formation, at least several plumes develop at the bottom. Therefore, the chosen aspect ratio does not significantly influence the fundamental aspects of the layer formation. The numerical discretization is 128×256 cells, which is based on extensive testing of the accuracy of the solutions by using various grids and varying the time step size.

4.3 Results

The main objective of this study is to understand the formation and evolution of vertically stacked convective layers in porous media. Therefore a number of calculations in a numerical presentation of a Hele-Shaw cell of aspect ratio $A = 0.5$ is performed with various values of Ra_T and R_ρ. First, the observations on the generation of several convective layers in one typical experiment are described in detail. The parameters in this experiment are $Ra_T = 10^5$ and $R_\rho = 3$. Next, the data are analyzed in order to understand what limits the height of the convective layers (section 4.3.2). In section 4.3.3, the sensitivity of the layer formation is studied as a function of parameters and initial conditions. Finally, two dynamical mechanisms are described, which cause intermittent changes in the vertical layer scale (section 4.3.4).

4.3.1 Layer formation

In Figure 4.2a-f the thermal, compositional and density distributions are shown at six different stages in the evolution. A light (dark) shading indicates a low (high) temperature or enriched (depleted) compositional concentration. Figures 4.2g-h display the corresponding vertical profiles of horizontally averaged temperature, composition, and density. In Figure 4.2h, a set of different density profiles are also displayed to provide an overview of the evolution of the layer formation.

Figure 4.2a and profiles i in 4.2g-h display a thin thermal boundary layer developing at the bottom. Due to the large temperature difference across this layer, it becomes unstable almost instantaneously. Several convective plumes rise from this boundary layer into the cold and compositionally lighter environment. Since heat diffuses faster than solute concentration, a plume loses its thermal buoyancy faster than it loses its solute. This results in a relatively heavy fluid in the plume, as compared to the environment. Consequently, the plume starts to sink again. The region near the bottom is rapidly mixed by the rising and sinking currents, leading to a chemically almost uniform layer with increasing temperature. The density distribution of the motionless fluid above the convective layer is still unaffected (see profiles i above the thick arrows). The rising plumes erode the initial density gradient by incorporating the nonbuoyant fluid into the convective layer. This mechanism, which we call 'convective entrainment', increases the layer thickness with time.

Figure 4.2b and profiles ii in 4.2g depict the situation a little later. A sharp density interface has developed on top of the convective plumes, hindering further entrainment. This stable, horizontal density interface arises from the jump in compositional concentration and separates the motionless fluid from the strongly convecting layer below the interface. The vast majority of the plumes are stopped by the interface, while only the most vigorous ones are able to entrain further some material from the upper layer. The plumes, which are almost stopped by the distorted interface, spread out horizontally. This results in the development of a highly deformed but joined interface between the well-mixed layer and the overlying fluid. Due to low compositional dispersion there is virtually no flux of solute across the interface. There is, however, a significant diffusive heat flux from the plume head through the interface into the upper layer. This heat flux is strong enough to destabilize the upper layer. Small plumes evolve initially on top of the plume heads which have evolved in the layer beneath (Figure 4.2b).

Convective mixing in the upper layer increases the compositional difference between both layers, while the diffusive heat flux across the interface reduces the temperature difference across the interface. Both processes lead to a further increase of the density difference $\Delta\hat{\rho}_{\text{int}}$ between both layers, affecting the further evolution in several ways.

As clearly visible in Figure 4.2h, the increasing density difference results in a flattening of the interface until an almost planar boundary has evolved. A further consequence of the increase of the density jump is that the growth rate of the first layer decreases with time. As mentioned above, a few vigorous plumes are still able to entrain material from above thus leading to further growth. With increasing $\Delta\hat{\rho}_{\mathrm{int}}$, however, fewer and fewer plumes can entrain material from above.

The thickness of the upper convective layer is influenced by two competing mechanisms. On the one hand, this layer grows by entraining fluid from above. Similar to the evolution of the first layer, a density interface develops on top of this layer and limits the amount of fluid that can be entrained. On the other hand, at least a few of the most vigorous plumes in the first layer can still penetrate the density interface between the two layers and entrain fluid from the upper layer into the first one. This mechanism evidently decreases the thickness of the upper layer, as its lower boundary layer migrates upwards.

Initially, the upper layer entrains more fluid from above than it loses fluid through the bottom, because the density jump on top of the upper layer is still very small. As a result, the thickness of the upper convective layer increases. When the density jump on top of this layer has increased sufficiently, the plumes in the upper layer cannot entrain fluid from above anymore (Figure 4.2c and profiles iii in 4.2 g-h). The fully developed convective upper layer then reaches its maximal height.

From that point on, the thickness of the upper convective layer decreases again, due to the erosion of this layer by the most vigorous plumes from the layer beneath (compare height of the upper layer, indicated in $\hat{T}$ profiles iii-iv with arrows u in Figure 4.2g-h). The entrained fluid is mixed with the fluid of the first layer (Figure 4.2d and profiles iv in 4.2 g-h). This process gradually decreases the density difference across the interface, which results in growing deflections of the interface. Ultimately, the interface can not be maintained and the upper convective layer merges into the lower one. From now on, we will call this small convective layer, which is finally entrained into the first one, the transient layer.

Meanwhile, another convective layer has developed on top of the transient layer. As mentioned before, these layers are also separated by a thin density interface. At the moment when the transient layer vanishes and the two lowest interfaces merge, the density difference across this newly formed interface increases significantly (see profiles v). From this moment, the growth rate of the first layer is virtually zero. Advective mixing of the fluid in the new top layer results in a compositionally uniform interior and sharp boundary layers. Subsequent layers are generated similarly. A stable density interface grows on top of each layer, thus preventing further entrainment. Heat transfer across the interface destabilizes the next layer.

Altogether, a staircase of well-mixed convecting layers develops, separated by thin density interfaces (see Figures 4.2e and 4.2f and profiles v-vi). Note that the lowermost layer is much thicker than all of the others. Finally, when the heat is sufficiently large to destabilize all fluid, the convective layers reach the top of the domain and the interfaces start to break down one after the other from the top down. Ultimately, one chemically homogeneous convective layer remains.

4.3.2 Self-limitation of the convective layers

One important question to answer is: what limits the convective layer to a certain height? In laboratory experiments on free flow, basically two mechanisms have been proposed to determine the thickness of a layer. Following *Turner* [1968], a stationary situation is reached when entrainment from below the interface by convection in the upper layer balances entrainment from above the interface by convection in the lower layer.

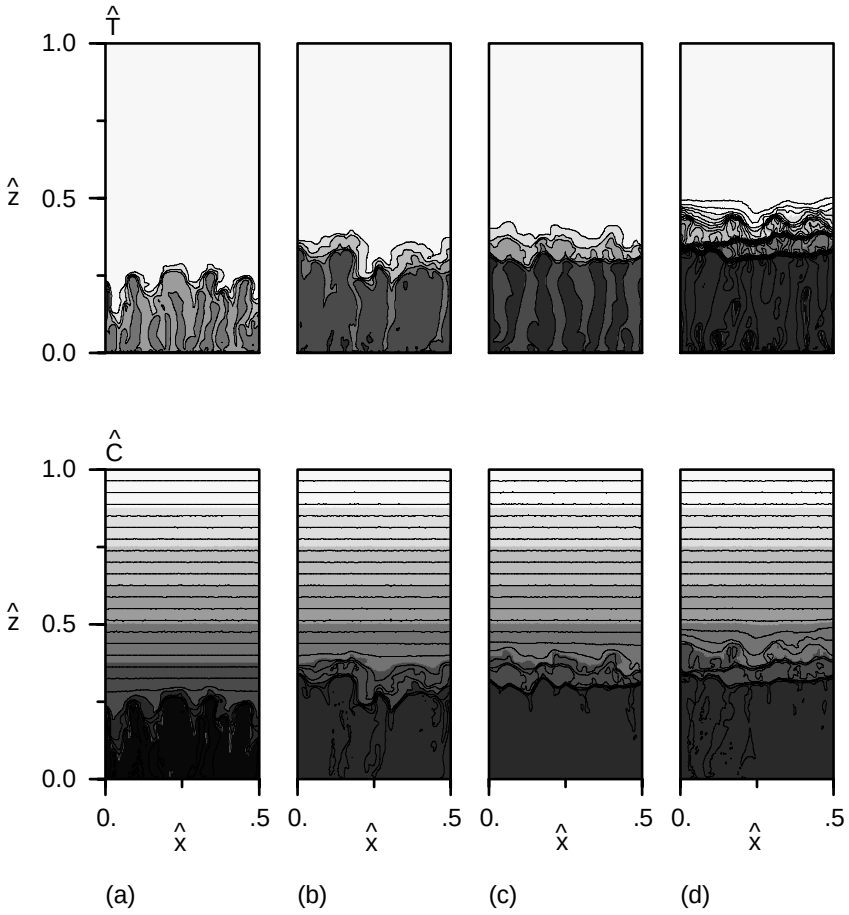

Figure 4.2: Snapshots of temperature $\hat{T}$ and compositional concentration $\hat{C}$ of a simulation with $Ra_T = 1 \times 10^5$, $R_\rho = 3$ and $Le = 100$, at (a) $\hat{t} = 0.000462$, (b) $\hat{t} = 0.001108$, (c) $\hat{t} = 0.001612$, (d) $\hat{t} = 0.002607$, (e) $\hat{t} = 0.005047$, and (f) $\hat{t} = 0.012491$. Light (dark) shading indicates low (high) temperature or enriched (depleted) compositional concentration. In the $\hat{C}$ snapshots and the $\hat{T}$ ones in panels d-f the interval is 0.033 (see legend). Contour interval in the $\hat{T}$ snapshots in panels a-c is 0.1, as to show more clearly the thermal evolution of the first layer. (g) Transient development of horizontally averaged profiles of $\hat{T}$ and $\hat{C}$ at the times corresponding to figures 4.2a-f. The arrows *u* indicate the upper (transient) convective layer. (h) Upper panel: density profiles $\hat{\rho}^* = \hat{\rho} - \hat{\rho}_0 = Ra_T(R_\rho \hat{C} - \hat{T})$. Lower panel: similar, but at many more times between $\hat{t} = 0.0$ and $\hat{t} = 0.015$. The development and sharpening of five interfaces is clearly shown. The thicker arrows in Figures 4.2g-h indicate the still stably stratified profile above the convective layer.

An alternative explanation for the substantial decrease in growth rate is proposed by *Fernando* [1987]. Due to the development of a buoyancy jump on top of the first mixed layer, plumes cannot penetrate through the compositional interfacial boundary layer and further entrain material from above. According to his experiment, turbulent entrainment is replaced by purely diffusive heat and mass transport across the interface, which leads to a sudden stop of the layer growth.

In order to investigate if and which one of these mechanisms is relevant in our case, we

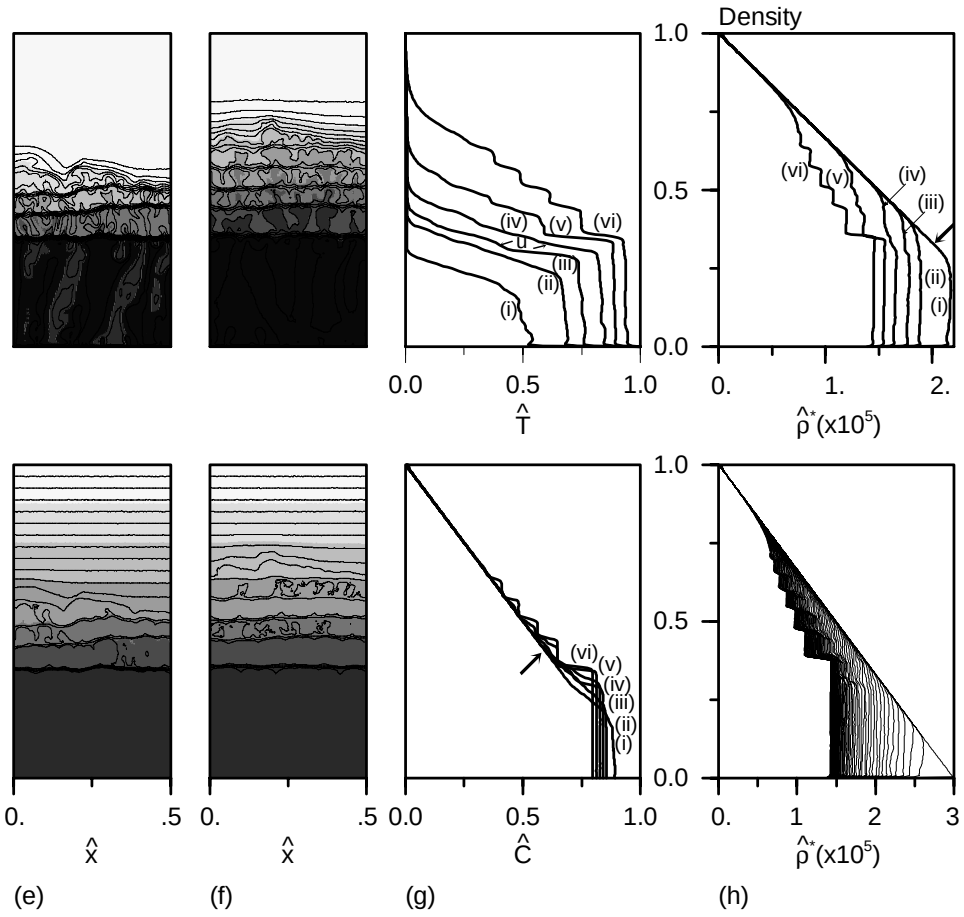

Figure 4.2: Continued.

have focused our attention on the evolution of the first-second layer system. The different stages can be summarized as follows (Figure 4.3): in the first phase the layer grows very fast by entraining fluid from above, while a density jump develops on top of the convective layer (from the start up to arrow 2). This is followed by a period of decreasing layer growth (stage confined between arrows 2 and 3). During this phase, the transient layer has developed on top of the first layer and is gradually eroded from below. Finally, after mixing of the first and transient layer, the thickness of the first layer remains unchanged (stage from arrow 3).

Since in our experiments a density jump clearly develops on top of the first layer, the mechanism as proposed by *Fernando* [1987] seems to be relevant at a first glance. However, the evolution of the first layer differs from pure viscous flow in several aspects. First, the decrease in growth rate is not as abrupt as in free flow. Secondly, other layers have developed on top of the first layer, before the first layer has reached its final depth. Therefore, also the mechanism of balanced entrainment, as proposed by *Turner* [1968], can play a role in determining the layer height. In order to distinguish between both mechanisms, we have monitored the transport properties near the interface. For the balanced entrainment mechanism to be relevant one expects a significant advective component of heat and mass flux, while the

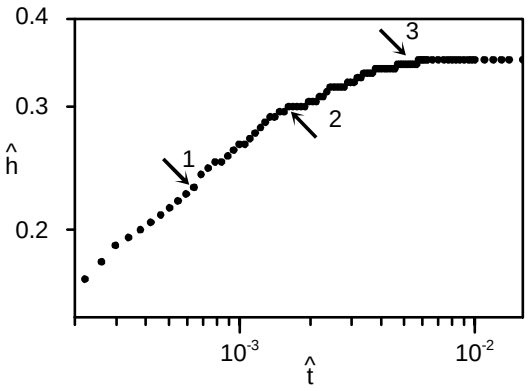

Figure 4.3: Temporal evolution of the height $\hat{h}$ of the first layer.

mechanism as proposed by *Fernando* [1987] is characterized by a purely diffusive/dispersive interfacial transport.

In dimensionless form, the horizontally averaged diffusive (dispersive) flux of heat (solute) is defined as

$$-\overline{\frac{\partial \hat{T}}{\partial \hat{z}}} \quad ; \quad -\overline{\frac{\partial \hat{C}}{\partial \hat{z}}} \tag{4.1}$$

and the advective flux as

$$\overline{\hat{w}\hat{T}} \quad ; \quad Le_{\text{eff}}\,\overline{\hat{w}\hat{C}/\phi^*}. \tag{4.2}$$

The results of the measurements are shown in Figure 4.4. Horizontally averaged fluxes are plotted at three time instants, corresponding to those marked in Figure 4.3. Each profile has been time averaged over a number of profiles around these time instants. As expected, in the well-mixed convecting layer the advective fluxes are much larger than the diffusive ones. Furthermore, the magnitude of the compositional advective flux is relatively larger than that of heat, because of the high *Le*. Note that this would even increase for a system with a low porosity ϕ.

At the first time instant (solid curves), the density interface on top of the first layer is highly contorted between $\hat{z} = 0.2$ and 0.3 (indicated by number 1 in the diffusive/dispersive flux profiles). Consequently, the horizontally averaged fluxes through this interface are smeared out between these two heights. Clearly, the advective components of both heat and solute fluxes dominate the transport on top of the convective layer. This indicates that fluid is advectively entrained from above into the first layer.

At the second time instant (dashed curves), the density difference between the first and transient layers has just reached its maximum value. Therefore the density interface between these layers is less deflected than at the previous time point. As a result, peaks can be observed in the diffusive flux profiles at the position of the first density interface ($\hat{z} = 0.30$, indicated by arrow 2), while a minimum value can be distinguished in the advective flux profiles. While the diffusive and advective components of the heat flux across the interface are of the same order, the advective component of the solute flux still dominates the dispersive one. This clearly indicates that entrainment across the interface has decreased, due to the increased

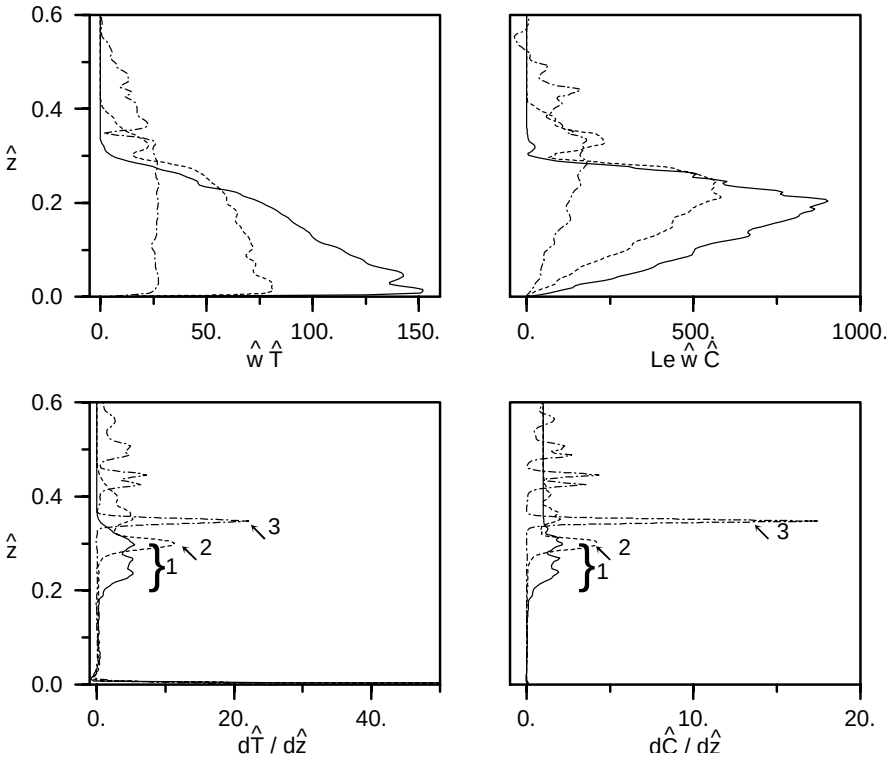

Figure 4.4: Horizontally averaged diffusive/dispersive and advective fluxes of T and C, as defined in (4.1) and (4.2), plotted as a function of depth at three stages in the evolution: $\hat{t} = 0.000640$ (solid curves), $\hat{t} = 0.001612$ (dashed), and $\hat{t} = 0.005047$ (dash-dotted). The numbered arrows indicate the position of the first interface in the diffusive/dispersive profiles at the three time instants.

density difference between the two adjacent layers. Nevertheless, the transient mixed layer can be entrained slowly into the lowermost layer.

Finally, the dash-dotted curves show the fluxes shortly after the transient layer has merged into the first mixed layer. The very sharp peaks in the diffusive profiles demonstrate the flatness of the interface (at $\hat{z} = 0.35$, indicated by arrow 3). At this stage, both heat and solute fluxes are diffusively dominated through this interface. Furthermore, total fluxes of both quantities are relatively small, as compared to the ones during the earlier stages.

The flux measurements reveal a transition from a regime in which convective entrainment dominates to a regime where the transport across the interface is purely diffusive/dispersive. These findings rule out the mechanism of balanced entrainment, as proposed by *Turner* [1968] for free flow. They seem to indicate that in fact the density jump limits the growth of the layer in porous media flow, just like in free flow [*Fernando,* 1987].

The gradual change toward a diffusively/dispersively controlled regime near the interface can, however, also indicate that a thermal equilibrium is reached and that this limits the layer growth. The convective flow in the lower layer would then resemble a statistically steady state, in which the horizontally averaged temperatures do not change anymore. Moreover, the fluxes through the horizontal boundary layers of the convective layer would be equal and, consequently, the layer growth stops. The flow does not really reach a statistically steady

state, because heat and mass transfer across the interface between the two adjacent layers erodes the density jump on a compositionally dispersive time scale. In the ultimate time limit, all interfaces will have disappeared and one chemically homogeneous convective layer will remain. In the following, we consider the evolution to a thermal equilibrium as the third mechanism which possibly limits the layer height.

One way to distinguish between the two latter mechanisms is by comparing the total flux of the driving component (temperature) through the horizontal boundary layers of the lowermost layer. For the second mechanism to be valid, the heat flux through the interface is still smaller than the bottom heat flux, at the stage when the layer growth stops. When the third mechanism limits the layer growth, both boundary layer heat fluxes just have become equal at this stage.

The heat fluxes through both boundary layers of the first convective layer are compared at the same three time instants as before. Heat flux through the bottom of this layer is always purely diffusive, because the bottom of the domain is impermeable. The diffusive heat flux through the bottom can be seen indirectly in Figure 4.4, from the advective heat flux profiles. At the position just above the bottom boundary layer, the advective heat flux is nearly equal to the bottom heat flux. At the first time instant (solid profiles) the bottom heat flux is equal to 150 dimensionless units, which is much larger than the total heat flux through the sharp density interface. During the stage of entrainment of the transient layer (dashed profiles) the bottom heat flux is approximately 80 dimensionless units, still twice as large as compared to the heat flux across the interface. At the moment when the layer growth stops (dash-dotted profiles), the thermal fluxes through bottom and interface are virtually identical.

Thus the fluxes across the two boundary layers of the first layer equalize gradually until they match at the point when the layer growth stops. In our view, the arrival at the thermal equilibrium is actually what limits the growth of the first convective layer. We therefore favor the third mechanism, as to determine the final thickness of this layer. In nearly the same period, the density jump on top of the layer becomes sufficiently strong to prohibit the plumes to entrain fluid from above. As a result, heat (mass) transfer across this interface becomes purely diffusive (dispersive). When the growth of the density jump would have occurred at a faster rate than the growth toward the thermal equilibrium, the mechanism of a transition in the entrainment regime near the interface would have determined the layer height, as is the case in free flow [*Molemaker and Dijkstra,* 1997].

4.3.3 Parameter dependence and initial conditions

In this section, the sensitivity of behavior of the layer-forming mechanism to the parameters and initial conditions is investigated. First, the behavior of the layer formation is studied as a function of the most important parameters starting with Ra_T, while the buoyancy ratio is fixed to $R_\rho = 3$. At relatively low Rayleigh numbers ($Ra_T < 2 \times 10^3$), thermal buoyancy is not sufficiently large to destabilize the bottom thermal boundary layer. Instead, vertical heat (solute) transfer remains purely diffusive (dispersive) throughout the medium. Equivalent findings were documented by *Rosenberg and Spera* [1992], who performed similar experiments for $Ra_T = 600$ at slightly lower *Le*. Note that after dispersive homogenization of the chemical field, the fluid will eventually destabilize when $Ra_T > 25\pi^2/4 \approx 62$ (which is the critical Rayleigh number for pure thermal convection, as derived with linear stability for an aspect ratio of 0.5).

For Rayleigh numbers in the range $2 \times 10^3 < Ra_T < 15 \times 10^3$, the boundary layer becomes unstable almost instantaneously and a convective layer with a density interface on top develops at the bottom (see $\hat{T}$ and $\hat{C}$ profiles i in Figure 4.5, for $Ra_T = 10^4$). The heat flux through

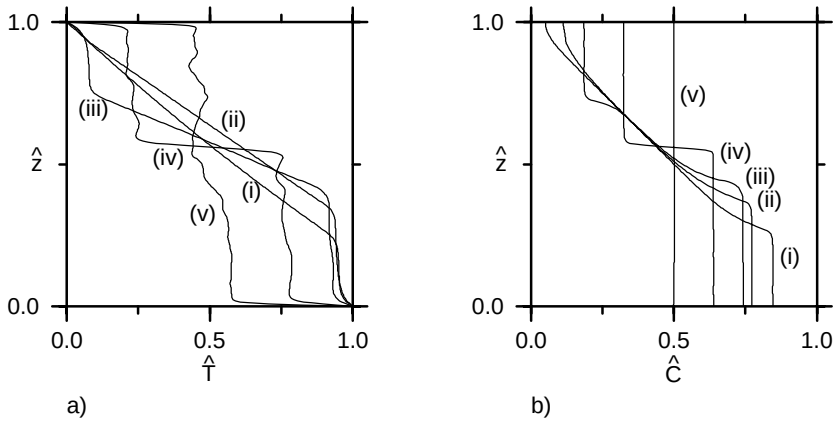

Figure 4.5: Transient development of horizontally averaged profiles of (a) $\hat{T}$ and (b) $\hat{C}$ at (i) $\hat{t} = 0.193451$, (ii) $\hat{t} = 0.958174$, (iii) $\hat{t} = 1.24493$, (iv) $\hat{t} = 1.522352$, and (v) $\hat{t} = 1.58901$. Here $Ra_T = 10^4$, $R_\rho = 3$, and $Le = 100$.

the interface is, however, not large enough to destabilize the fluid above. Eventually, after dispersive homogenization of the chemical field, the fluid also destabilizes near the no-flux top boundary such forming another convective layer (profiles ii). These two convective layers grow vertically toward each other, by dispersive entrainment of the non-buoyant intermediate fluid (profiles iii). This leads to a system in which two convective layers are separated by a thin diffusive/dispersive interface (profiles iv). Ultimately, after breakdown of this interface by one of the mechanisms described in the next section, one chemically homogeneous convective layer remains (profiles v). Note that the characteristic amount of time needed for the layer formation is now determined by the dispersive entrainment of nonbuoyant fluid into the layers.

At even larger Ra_T, multiple layers are generated in the way as described in section 3.1. The number of layers that form increases with increasing Ra_T. It is interesting to note that the frequency of breakdown of newly formed interfaces above the lowermost one is also higher at larger Rayleigh numbers.

Figure 4.6a shows the final thickness of the first layer $\hat{h}_f$ as a function of Ra_T for four simulations in this multiple layer regime. The results indicate that a power law relation exists between $\hat{h}_f$ and Ra_T, with an exponent of 0.14. The low sensibility of the layer thickness on Ra_T implies that the amount of fluid, which is entrained from above, mainly depends on the ratio of driving (thermal) and stabilizing (chemical) buoyancy. Since R_ρ is fixed, this ratio does not change when the thermal Rayleigh number increases. Intuitively, the weak dependence between $\hat{h}_f$ and Ra_T points out that at a given R_ρ a Rayleigh number exists above which the first layer contains the whole domain. For $R_\rho = 3$, the necessary Rayleigh number would be of the order of $O(10^8)$. Runs with these parameters can, however, not be resolved in this study.

Figure 4.6b displays the dependence of $\hat{h}_f$ on the other essential parameter R_ρ, while the Rayleigh number is kept at $Ra_T = 10^5$. A simple power law that describes the data is

$$\hat{h}_f = 0.9\, R_\rho^{-1.0}. \tag{4.3}$$

Thus the layer thickness is inversely proportional to the overall buoyancy ratio R_ρ.

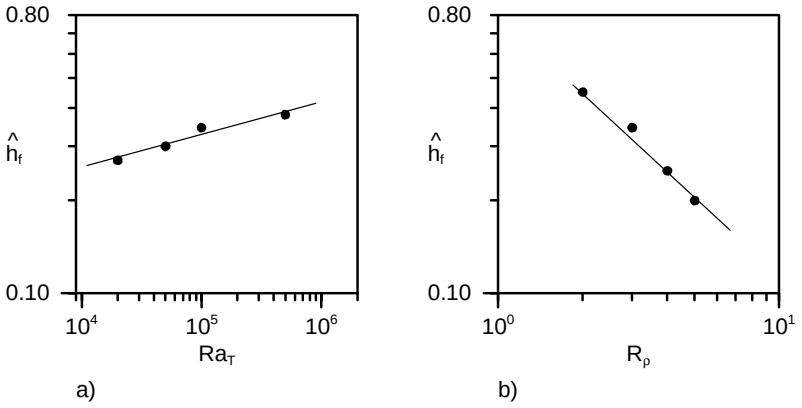

Figure 4.6: (a) The final layer height of the first layer $\hat{h}_f$ as a function of Ra_T for a constant buoyancy ratio $R_\rho = 3$ for $\phi = 1$. (b) The final layer height $\hat{h}_f$, but now as a function of R_ρ, while the Rayleigh number is fixed to $Ra_T = 10^5$ and porosity to $\phi = 1$.

This strong relationship could suggest that a simple explanation exists for the determination of the layer height, which is just the estimation of how high a parcel of fluid from the bottom of the domain can rise before its density becomes equal to that expected from the initial conditions. This would also predict a final layer thickness of $1/R_\rho$. Since the layer thickness gradually changes with Ra_T (see Figure 4.6a), however, the arrival at the thermal equilibrium is sustained as the criterion for limitation of the layer growth.

Alternatively to an initially cold system, in many natural systems the geotherm increases gradually with depth. Therefore we have applied a linear temperature profile, on which a small perturbation of the form $10^{-3}\cos(2\pi\hat{x})\sin(\pi\hat{z})$ is superposed to start away from a nonphysically stable point. Porosity is equal to $\phi = 1$ again. The buoyancy ratio is fixed at $R_\rho = 2$, while the Rayleigh number is varied.

For Rayleigh numbers up to $Ra_T = 25\pi^2/4$, the fluid does not destabilize. Instead, the system evolves statically toward its final state of a conductive and chemically homogeneous domain. When $Ra_T > 25\pi^2/4$, a number of stages can be identified. Initially, the fluid also remains motionless (see $\hat{T}$ and $\hat{C}$ profiles i in Figure 4.7 for a run with $Ra_T = 4\times10^4$). During this period, the initially stably stratified density profile erodes dispersively at the top and bottom of the domain. When the stability has decreased sufficiently, the fluid destabilizes near these sides.

From this point the system evolves in three different ways, dependent on the value of Ra_T. For $25\pi^2/4 < Ra_T < 10^3$, the destabilization of the fluid near the two sides leads to the formation of a single convective layer across the whole domain. When $10^3 < Ra_T < 3\times10^4$, two separately convecting layers develop, one at each horizontal side of the domain. These layers grow vertically by dispersive entrainment of intermediate fluid, meet each other and, ultimately, merge to form one chemically homogeneous convective layer. Finally, for $Ra_T > 3\times10^4$ at first convective layers develop at both sides again, which grow by the entrainment of fluid from the interior (profiles ii). After the layers have grown substantially, however, the intermediate fluid destabilizes separately such leading to three or more vertically stacked convective layers (profiles iii-iv). These layers eventually merge after breakdown of the density interfaces. Ultimately, one well-mixed convective layer remains (profiles v).

To conclude, layers can be generated under conditions different than those described in

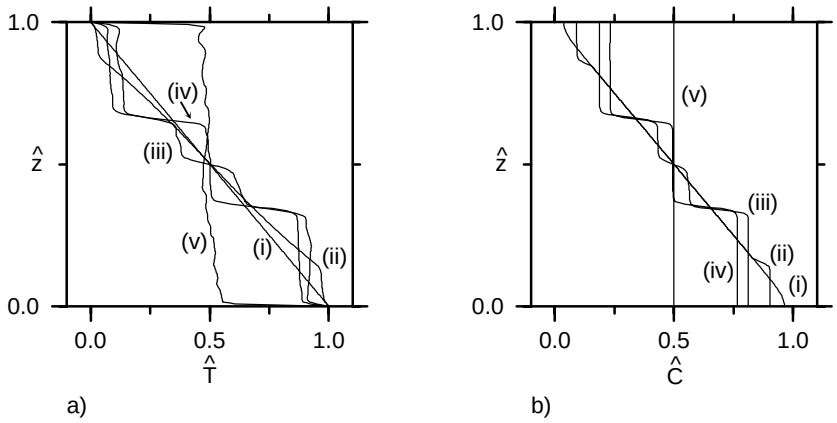

Figure 4.7: Transient development of horizontally averaged profiles of (a) T and (b) C, starting from a linear temperature field. Parameters are $Ra_T = 4 \times 10^4$, $R_\rho = 2$, and $Le = 100$. The corresponding times are (i) $\hat{t} = 0.136530$, (ii) $\hat{t} = 0.330819$, (iii) $\hat{t} = 0.588555$, (iv) $\hat{t} = 0.603311$, and (v) $\hat{t} = 0.624103$.

the previous sections. Starting with a linear temperature profile, convective layers develop only after considerable dispersive homogenization of the initially stably stratified chemical field. The evolution from a relatively large and sharp temperature contrast is therefore a more robust and rapid mechanism to produce layered structures. Layers are formed on a thermally advective time scale. While the number of layers that develop is determined by the magnitude of the thermal Rayleigh number, the final height of a newly formed layer is inversely proportional to the buoyancy ratio.

4.3.4 Intermittent changes of layer structures

Ultimately, at least on a compositionally dispersive time scale, all interfaces will have vanished and the fluid will be chemically homogeneous. On a much shorter time scale, the breakdown of an interface followed by a partial homogenization can take place by dynamical mechanisms. Within the set of experiments we have observed several interfaces vanishing. In most cases the lowest interface in the domain has vanished, but also intermediate ones did disappear. Two mechanisms have been observed, by which the two surrounding convective layers merged. Both mechanisms are elucidated by a few close-up snapshots of $\hat{T}$ and $\hat{C}$ from another experiment ($Ra_T = 5 \times 10^5$ and $R_\rho = 3$).

In Figure 4.8a, a planar interface can be observed between the lowermost and second layer (at $\hat{z} = 0.21$, indicated by the arrow). This density interface 'migrates' slowly upwards (Figures 4.8a and 4.8b). Apparently, fluid from the second layer is entrained into the first one. Since the height of the next interface remains fixed at $\hat{z} = 0.255$, the thickness of the second layer decreases. Although the solute contrast between these two layers decreases by the entrainment, the density jump across the interface does not change significantly. Therefore any deflection of the interface experiences a strong restoring force, keeping the interface planar. When the effective thermal Rayleigh number (defined as $Ra_{T,\mathrm{eff}} = \alpha K \rho g \Delta T_l h_l / \kappa \mu$, where h_l is the height of the layer and ΔT_l the effective temperature drop across the layer) becomes subcritical, convection in the upper layer ceases (Figure 4.8c). Finally, the two density interfaces merge, and a single, high-density interface develops between the lowermost and the new top layer (Figure 4.8d).

A similar upward migration of a density interface was observed in laboratory experiments on free flow [*Huppert and Linden,* 1979] and on flow in porous media [*Griffiths,* 1981]. According to *Fernando* [1989], two conditions must be met for the interface to migrate. First, convection in the lower layer should be stronger than in the upper layer, and, second, the density difference across the interface should be sufficiently low to allow for advective entrainment.

In our experiments on porous media flow, the first condition is clearly met. While the temperature drop across both individual layers is almost the same, the depth extension of the lower layer is about 4 times larger than the depth of the upper layer. This translates into a local Ra_T, which is likewise 4 times larger in the lower than in the upper layer. Convection is therefore more vigorous in the lower layer than in the upper one and the condition as mentioned above is met. The validity of the second condition for porous media flow is not investigated here, but will addressed explicitly in the next chapter.

Besides the upward migration of an interface, we have observed a further mechanism leading to the destruction of an interface. In the same experiment at a later time instant, an initially planar interface at $\hat{z} = 0.50$ exhibits growing deflections (Figure 4.9a-4.9c), until it reaches the interface above. At this point, the interface 'breaks down' and the two adjacent layers merge vigorously (Figures 4.9d and 4.9e). Also this type of mechanism was observed for free flow [*Huppert and Linden,* 1979] and was interpreted by *Griffiths* [1981] for flow in porous media.

Griffiths [1981] showed, that the amplitude of the interface distortions depends on the buoyancy ratio across the interface $R_{\rho\,\mathrm{int}} = \beta\Delta C_{\mathrm{int}}/\alpha\Delta T_{\mathrm{int}}$, where ΔC_{int} and ΔT_{int} are the chemical and thermal differences across the interface. The amplitudes of the deflections were of the order of the horizontal cell size, when the buoyancy ratio across the interface was in the range $2.3 < R_{\rho\,\mathrm{int}} < 3$. He proposed that at even lower $R_{\rho\,\mathrm{int}}$ the deflections become so large that the interface touches the interface above and breaks down.

In order to compare our findings with Griffiths' results, we have checked the buoyancy ratios across the interface. At the stage when the deflections are very small (Figure 4.9a), the buoyancy ratio across the interface is $R_{\rho\,int} \approx 1.4$. This value is obtained by taking the horizontal mean of $R_{\rho\,\mathrm{int}}$. At the moment when the interface touches the interface above (Figure 4.9c), the buoyancy ratio has decreased to $R_{\rho\,\mathrm{int}} \approx 1.1$. Since at this stage the deflections are very large, a horizontal average does not show an appropriate value for $R_{\rho\,\mathrm{int}}$. As an alternative, the buoyancy ratio is measured at a few single lateral positions. The value of 1.1 is obtained by averaging these different values. In accordance with Griffiths' results, we find the magnitude of the deflections dependent on the buoyancy ratio across the interface, but at typically lower values of $R_{\rho\,\mathrm{int}}$. The discrepancy between Griffiths' and our values for $R_{\rho\,\mathrm{int}}$ might arise from the assumption that chemical dispersion in the solid and liquid are equal.

Naturally, vanishing of interfaces by the 'migration' and convective 'breakdown' mechanisms alters the thickness of the individual layers during time. These intermittent changes in the layer structures determine the vertical scales of the convective layers, rather than the initial evolution toward a thermal equilibrium.

4.4 Summary

The formation and evolution of horizontally layered structures has been investigated with a numerical model of the convection in a Hele-Shaw cell, in which a temperature contrast is imposed at the bottom of a compositionally stably stratified fluid. It is shown that double-diffusive convection is a vital mechanism for the generation of layered structures. Instabilities

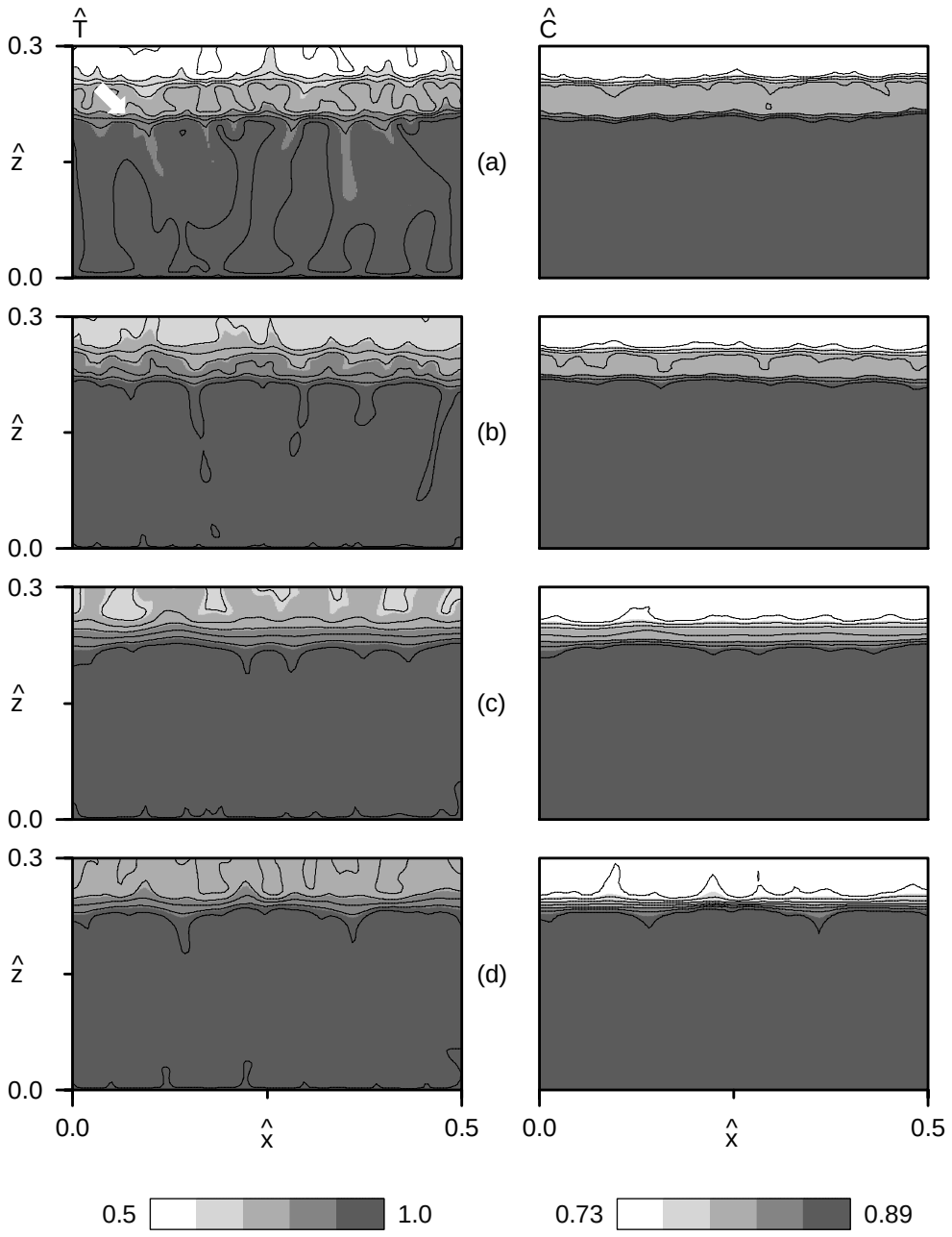

Figure 4.8: Close-up snapshots of $\hat{T}$ and $\hat{C}$ for $Ra_T = 5\times10^5$, $R_\rho = 3$, and $Le = 100$. The corresponding times are (a) $\hat{t} = 0.005255$, (b) $\hat{t} = 0.010048$, (c) $\hat{t} = 0.012887$, and (d) $\hat{t} = 0.015451$. The interface between the first and second layer (indicated by the arrow in panel (a) 'migrates' slowly upwards, due to a difference in the vigor of convection between the two adjacent layers. In panels (c), the effective Rayleigh number of the upper convective layer becomes subcritical. As a result, convection in the upper layer stops and the two interfaces merge together.

which rise from the heated surface form a well-mixed convective layer at the bottom. This layer grows by further entrainment of material from above. Between the plume heads and the overlying fluid a sharp, stable density interface develops. The stability of the density jump arises from the difference in solute content between the convective layer and the motionless fluid above the interface. While low solute flux across the interface keeps the interface intact, heat flux destabilizes the overlying fluid. Subsequent layers are generated in a similar way, provided that the heat flux is large enough to destabilize the fluid above. In this way, a staircase of convective layers develops, separated by sharp diffusive/dispersive interfaces. Here we note that in all experiments the lower layer is much thicker than all of the others.

In our configuration the limitation of the first layer to a certain depth is neither a consequence of destabilization of the next layer, nor forced by the development of the density interface on top of the layer. Instead, the convective layer evolves to a thermal equilibrium, and the depth of the layer is determined by the amount of material which can be entrained within this period.

In that sense our results differ from those on viscous flow [*Turner,* 1968; *Fernando,* 1987; *Molemaker and Dijkstra,* 1997], where the layer height is limited by the formation of a sufficiently strong buoyancy jump before the thermal equilibrium is reached. Apparently, flow in porous media evolves faster toward a thermal equilibrium than in pure viscous flow. We attribute this difference to fundamental differences in the dynamical behavior of free viscous flow and flow in porous media. In the latter, both inertia and viscous coupling are negligible, thus leading to narrow convection cells [*Rosenberg and Spera,* 1992]. The vertical advective transport of heat and solute works very efficiently within these cells, such that the thermal equilibrium is reached faster than in free flow.

We also note that in the mentioned laboratory and numerical work on free viscous flow a constant heat flux has been supplied at the boundary, while we have employed constant temperature conditions. In how far the behavior is influenced by the different boundary conditions needs further clarification.

Once it got established, an interface was observed to vanish through three mechanisms. Besides (1) the ultimate disappearance of any interface through diffusional homogenization, our experiments have shown that on short time scales (2) the 'migration' of an interface and (3) the 'breakdown' of an interface can lead to sudden changes of the layer structure. On a time scale short as compared to the dispersive one, interface migration and breakdown are the key mechanisms determining the layered structure, rather than the initial growth towards thermal equilibrium.

From the whole set of experiments which was performed in the course of this study, we have the following indications with respect to parameter dependence. First, the number of layers that develops is determined by the thermal Rayleigh number, while it is not very sensitive to the buoyancy ratio. Next, the thickness of a newly formed layer is inversely proportional to the buoyancy ratio, while its dependence on the thermal Rayleigh number is small. A staircase of convecting layers separated by thin density interfaces develops, in which the lowermost layer is the thickest again. Therefore the layer-generating mechanism as described here is also applicable to low-porosity systems. It is speculated, however, that a transition in the entrainment regime determines the limitation of the layer growth, rather than the arrival at a thermal equilibrium.

Layers do also form in systems with an initially linear temperature profile. However, the layer growth is determined by dispersive, rather than advective entrainment of fluid from the interior. Consequently, the layers are formed on a much larger time scale, as compared to the case in which a temperature contrast is applied at the bottom.

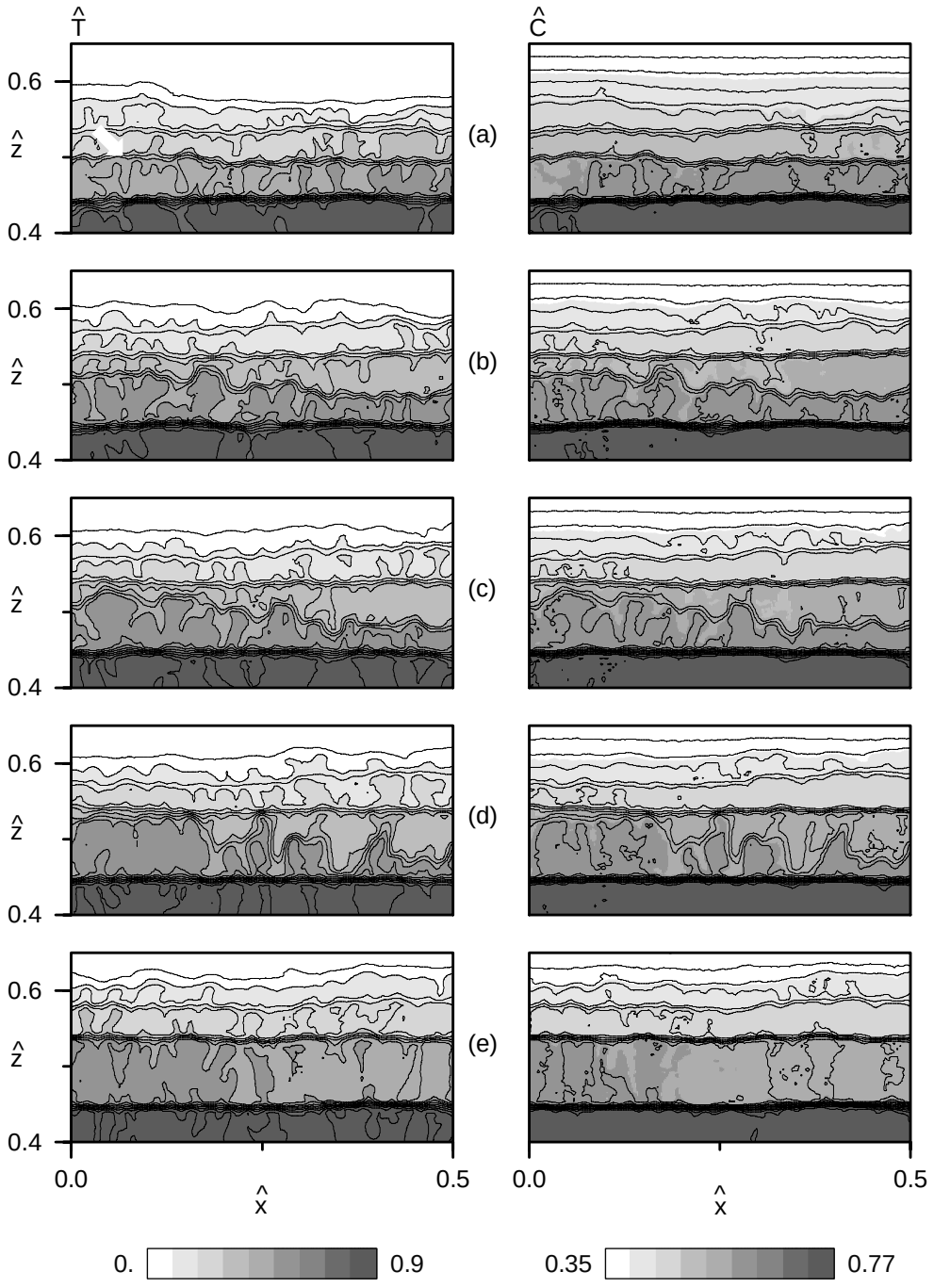

Figure 4.9: Close-up view of $\hat{T}$ and $\hat{C}$ at a later stage in the same experiment as shown in Figure 4.5: (a) $\hat{t} = 0.002767$, (b) $\hat{t} = 0.003055$, (c) $\hat{t} = 0.003116$, (d) $\hat{t} = 0.003177$, and (e) $\hat{t} = 0.003367$. Focus is on the interface between the second and third layer (indicated by the arrow in panel (a). This interface 'breaks down' because it touches the interface above.